UC Davis
UC Davis Previously Published Works

Title

Arabidopsis HIPP27 is a host susceptibility gene for the beet cyst nematode Heterodera schachtii

Permalink

Journal

ISSN

Authors

Radakovic, Zoran S
Anjam, Muhammad Shahzad
Escobar, Elizabeth
et al.

Publication Date

DOI

Peer reviewed

Arabidopsis *HIPP27* is a host susceptibility gene for the beet cyst nematode *Heterodera schachtii*

ZORAN S. RADAKOVIC[1], MUHAMMAD SHAHZAD ANJAM[1], ELIZABETH ESCOBAR[1],
DIVYKRITI CHOPRA[1], JAVIER CABRERA[2], ANA CLÁUDIA SILVA[2], CAROLINA ESCOBAR[2],
MIROSLAW SOBCZAK[3], FLORIAN M. W. GRUNDLER[1] AND SHAHID SIDDIQUE [1],*

[1]INRES–Molecular Phytomedicine, Rheinische-Friedrich-Wilhelms-University of Bonn, D-53115 Bonn, Germany
[2]Facultad de Ciencias Ambientales y Bioquímica, Universidad de Castilla-La Mancha, Área de Fisiología Vegetal, Avda, Carlos III, s/n, 45071 Toledo, Spain
[3]Department of Botany, Warsaw University of Life Sciences, PL-02787 Warsaw, Poland

SUMMARY

Sedentary plant-parasitic cyst nematodes are obligate biotrophs that infect the roots of their host plant. Their parasitism is based on the modification of root cells to form a hypermetabolic syncytium from which the nematodes draw their nutrients. The aim of this study was to identify nematode susceptibility genes in *Arabidopsis thaliana* and to characterize their roles in supporting the parasitism of *Heterodera schachtii*. By selecting genes that were most strongly upregulated in response to cyst nematode infection, we identified HIPP27 (*H*EAVY METAL-ASSOCIATED *I*SOPRE-NYLATED *P*LANT *P*ROTEIN *27*) as a host susceptibility factor required for beet cyst nematode infection and development. Detailed expression analysis revealed that HIPP27 is a cytoplasmic protein and that *HIPP27* is strongly expressed in leaves, young roots and nematode-induced syncytia. Loss-of-function Arabidopsis *hipp27* mutants exhibited severely reduced susceptibility to *H. schachtii* and abnormal starch accumulation in syncytial and peridermal plastids. Our results suggest that *HIPP27* is a susceptibility gene in Arabidopsis whose loss of function reduces plant susceptibility to cyst nematode infection without increasing the susceptibility to other pathogens or negatively affecting the plant phenotype.

Keywords: cyst nematode, *Heterodera schachtii*, HIPP27, plant-parasitic nematodes, starch, susceptibility gene, syncytium.

INTRODUCTION

Cyst nematodes are obligate biotrophs that cause extensive yield losses in almost all economically important crops (Jones *et al.*, 2013). The lifecycle of the cyst nematode begins when an infective-stage juvenile invades the root, preferentially in the elongation zone. Once inside the root, the juvenile beet cyst nematode travels through various tissue layers until it reaches the vascular cylinder, where it selects a single cell that will become the initial syncytial cell (ISC; Wyss and Zunke, 1986). On selection of the ISC, the nematode becomes immobile and releases proteinaceous and non-proteinaceous secretions inside the ISC to promote the formation and function of the syncytium (Gardner *et al.*, 2015; Habash *et al.*, 2017; Hewezi *et al.*, 2015; Siddique *et al.*, 2015). The syncytium is a metabolic sink and serves as the nematode's only source of nutrients for the remainder of its lifecycle. A plethora of metabolic, proteomic and transcriptomic changes accompany the development of the syncytium (Elashry *et al.*, 2013; Hofmann *et al.*, 2010; Hütten *et al.*, 2015; Siddique *et al.*, 2014a; Szakasits *et al.*, 2009). As the syncytium expands, the nematode differentiates into either a male or female (Trudgill, 1967). Although the mechanism of sex determination is not yet fully understood, host factors, such as defence activation and nutrient availability, influence the sexual outcomes of cyst nematodes (Mendy *et al.*, 2017; Shah *et al.*, 2017; Siddique *et al.*, 2014b, 2015). When there is a surplus of nutrients, more females develop. However, most nematodes develop into males under stress conditions, such as those in resistant plants.

A previous transcriptome analysis has shown that expression of a HEAVY METAL-ASSOCIATED ISOPRENYLATED PLANT PROTEIN (HIPP) family gene, *HIPP27*, is strongly upregulated in syncytia induced by the beet cyst nematode *Heterodera schachtii* in Arabidopsis roots (Szakasits *et al.*, 2009). Both prokaryotes and eukaryotes have evolved mechanisms to maintain efficient metal homeostasis inside the cell, including the presence of numerous metal transport proteins, known as metallochaperones. Most metallochaperones contain a heavy metal-binding domain (HMA; pfam00403.6) with a highly conserved CysXXCys motif and a $\beta\alpha\beta\beta\alpha\beta$-fold structure for binding Cu^+, Cd^{2+} or Zn^{2+} (Tehseen *et al.*, 2010). Many different families of metallochaperones function in plant defences against the toxicity of metals, such as cadmium, chromium and aluminium. In addition, several plant immune receptors carry HMA domains, indicating that HMA probably plays a role in plant defence against pathogens (Sarris *et al.*, 2016).

In addition to the HMA domain, members of the large HIPP family contain a C-terminal isoprenylation motif. HIPPs are present

Correspondence: Email: siddique@uni-bonn.de

only in vascular plants and are involved in a variety of biological processes, including heavy metal homeostasis and detoxification (Tehseen *et al.*, 2010), transcriptional responses to abiotic stresses, such as drought and cold (Barth *et al.*, 2009), and plant–pathogen interactions (de Abreu-Neto *et al.*, 2013; Zschiesche *et al.*, 2015). However, the mechanistic details underlying the roles of HIPPs in these biological processes remain mostly unknown. In *A. thaliana*, HIPPs make up the largest metallochaperone family, comprising 45 members divided into seven distinct classes (Tehseen *et al.*, 2010). The best-characterized member of this family in Arabidopsis is HIPP3, a zinc-binding protein that functions as an upstream regulator of the salicylate-dependent pathway during pathogen infection (Zschiesche *et al.*, 2015). As described above, the expression of *HIPP27* is strongly upregulated in syncytia induced by *H. schachtii* in Arabidopsis roots. Therefore, we hypothesized that HIPP27 might be an important host susceptibility factor in beet cyst nematode parasitism. In the present study, we investigated the role of HIPP27 in the interaction between *H. schachtii* and Arabidopsis. Our data show that *HIPP27* facilitates cyst nematode infection and the efficient development of nematode feeding sites in Arabidopsis roots.

RESULTS AND DISCUSSION

Selection of *HIPP27* as a candidate Arabidopsis host susceptibility gene for *H. schachtii*

The main objective of this study was to identify new target genes that could play a role in the susceptibility of Arabidopsis to *H. schachtii*. We mined previously published transcriptomic data and selected the top 100 genes that were most strongly upregulated in the syncytium compared with uninfected control roots (Szakasits *et al.*, 2009). We then performed a literature search, and all genes that played a role in crucial metabolic processes, such as photosynthesis and sugar metabolism, were excluded. This step was aimed at minimizing the risk of the selection of genes for which the loss-of-function mutant may show severe growth phenotypes. We also eliminated all genes whose loss-of-function mutants have been shown previously to exhibit severe root or shoot phenotypes. Next, BLAST searches were used to identify candidate genes for which only a single-copy orthologue was present in the genome of the natural host of *H. schachtii*, i.e. *Beta vulgaris* (Dohm *et al.*, 2014). Using this process, we ultimately selected 10 candidate host susceptibility genes (Table 1). The expression of these genes was validated in Arabidopsis plants that were grown *in vitro* and infected with *H. schachtii*. RNA was extracted from hand-dissected root segments containing syncytia that were sampled at 15 days post-infection (dpi), and was used to analyse the expression of the candidate genes via quantitative reverse transcription-polymerase chain reaction (qRT-PCR). The results confirmed that, of the 10 candidate genes, the expression

Table 1 Validation of the expression of 10 selected candidate genes in syncytia induced in Arabidopsis roots by beet cyst nematode.

Gene	Locus	Fold change compared with uninfected control	
		Microarrays (5 + 15 dpi)	qRT-PCR (15 dpi)
ENH1	AT5G17170	27.9	3.7 ± 0.26
UGP2	AT5G17310	29.9	2.6 ± 0.56
–	AT4G24830	29.9	3.3 ± 0.59
IMD2	AT1G80560	32.0	7.3 ± 4.7
NPC6	AT3G48610	39.3	30.0 ± 11.6
AD11A3	AT2G24270	48.5	44.5 ± 16.9
TRX1	AT3G51030	48.5	11.2 ± 3.28
CCR2	AT1G80820	52.0	15.47 ± 3.48
FAD6	AT4G30950	52.0	5.04 ± 1.71
HIPP27	AT5G66110	68.6	24.81 ± 2.88

For microarrays, data from microaspirated syncytia at 5 and 15 days post-infection (dpi) were pooled and compared with control roots (Szakasits et al., 2009). For quantitative reverse transcription-polymerase chain reaction (qRT-PCR), values represent the relative fold change in infected root segment containing syncytia relative to control uninfected root. 18S and UBP22 were used as housekeeping genes to normalize the data. All values are the means of three biological replicates ± standard error (SE)

of nine genes was upregulated (Table 1). However, the intensity of fold change was substantially lower than in the microarray data. This discrepancy between the qPCR and microarray data can probably be attributed to the different syncytial material used in the two cases: whereas microaspirated syncytial cell contents were used for microarray analysis, our qRT-PCR analysis was performed using cut syncytia containing the surrounding non-syncytial root cells, which may have diluted syncytium-specific mRNA expression.

We obtained loss-of-function homozygous mutants for the 10 candidate genes and analysed them for beet cyst nematode susceptibility via preliminary pathogenicity assays (Fig. S1, see Supporting Information). Amongst these, a mutant for the candidate gene *HIPP27* showed a particularly significant decrease in susceptibility to beet cyst nematode and was therefore selected for further molecular characterization.

HIPP27 is strongly upregulated in the syncytium

To investigate the expression patterns of *HIPP27* in various organs of Arabidopsis plants, we cloned the putative promoter region (472 bp) upstream of the translation start codon of *HIPP27*, producing the *pHIPP27:GUS* construct. Arabidopsis plants were transformed with *pHIPP27:GUS* and three independent homozygous lines were obtained. The general expression pattern of *pHIPP27:GUS* was then assessed in various plant organs. For uninfected lines, β-glucuronidase (GUS) staining was detected ubiquitously in all tissues examined, with particularly strong expression in young leaves (Fig. 1A–C). GUS expression was observed occasionally in uninfected roots, particularly in the
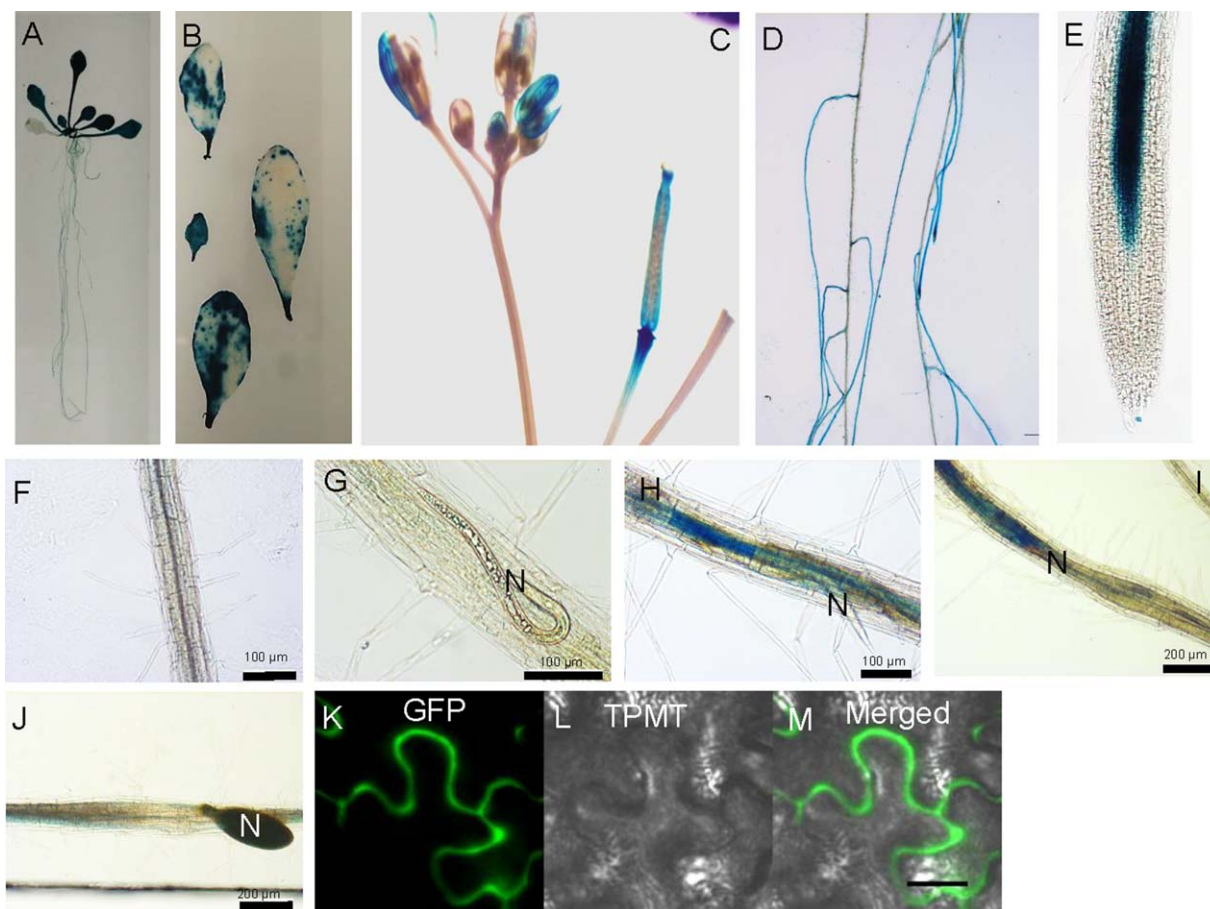
Fig. 1 *HIPP27* is strongly upregulated in the syncytium. Expression of *pHIPP27:GUS* in various organs of Arabidopsis: (A) 14-day-old seedling; (B) leaves from 2–3-week-old plants; (C) inflorescence; (D–F) 12-day-old root (0 days post-infection, dpi); (G–J) nematode-infected root segments at 1 dpi (G), 3 dpi (H), 5 dpi (I) and 10 dpi (J); (K–M) localization of *35S:HIPP27-GFP* in the epidermis of *Nicotiana benthamiana* leaves at 3 days after infiltration. N, nematode. GFP, green fluorescent protein; TPMT, Transmitted light detector.

younger parts (Fig. 1D,E); however, no staining was detected in the primary root, elongation zone and in the root tips (Fig. 1E,F). Plants harbouring *pHIPP27:GUS* were then infected with nematodes and stained for GUS activity at different time points after infection, i.e. 1, 3, 5 and 10 dpi, to cover the different stages of nematode development (Fig. 1G–J). We detected strong GUS expression at 3 dpi (Fig. 1H), which became intense at 5 dpi (Fig. 1I). However, GUS staining was either absent or only faintly detected at 10 dpi (Fig. 1J). GUS expression was generally localized inside the syncytium and extended beyond the syncytium in only a few cases, indicating that the upregulation of *HIPP27* is specific to nematode infection.

To determine the subcellular localization of HIPP27, HIPP27-GFP was transiently expressed in *Nicotiana benthamiana* leaf epidermis under the control of a constitutive promoter (CaMV 2x35S), and its localization was assessed using confocal microscopy. HIPP27-GFP was localized to the cytosolic region of the cell (Fig. 1J–L). Taken together, these results indicate that HIPP27 is a

cytoplasm-localized protein and that *HIPP27* expression is strongly upregulated during the early stages of syncytium development. These findings point to the likelihood of importance of this gene in early syncytium development.

Loss of function of *HIPP27* decreases Arabidopsis susceptibility to *H. schachtii*

To further substantiate the role of HIPP27 in the plant's interaction with cyst nematodes, we obtained two loss-of-function T-DNA insertion mutants of *HIPP27* (*hipp27a* and *hipp27b*; Fig. S2, see Supporting Information). Homozygous lines were selected after genotyping and the lack of *HIPP27* expression in the homozygous mutants was confirmed by RT-PCR (Fig. S3, see Supporting Information). To determine whether *hipp27* mutants showed any impairment in growth and development, we analysed phenotypic parameters in plants grown under sterile and glasshouse conditions for *hipp27a*. However, we did not observe any significant
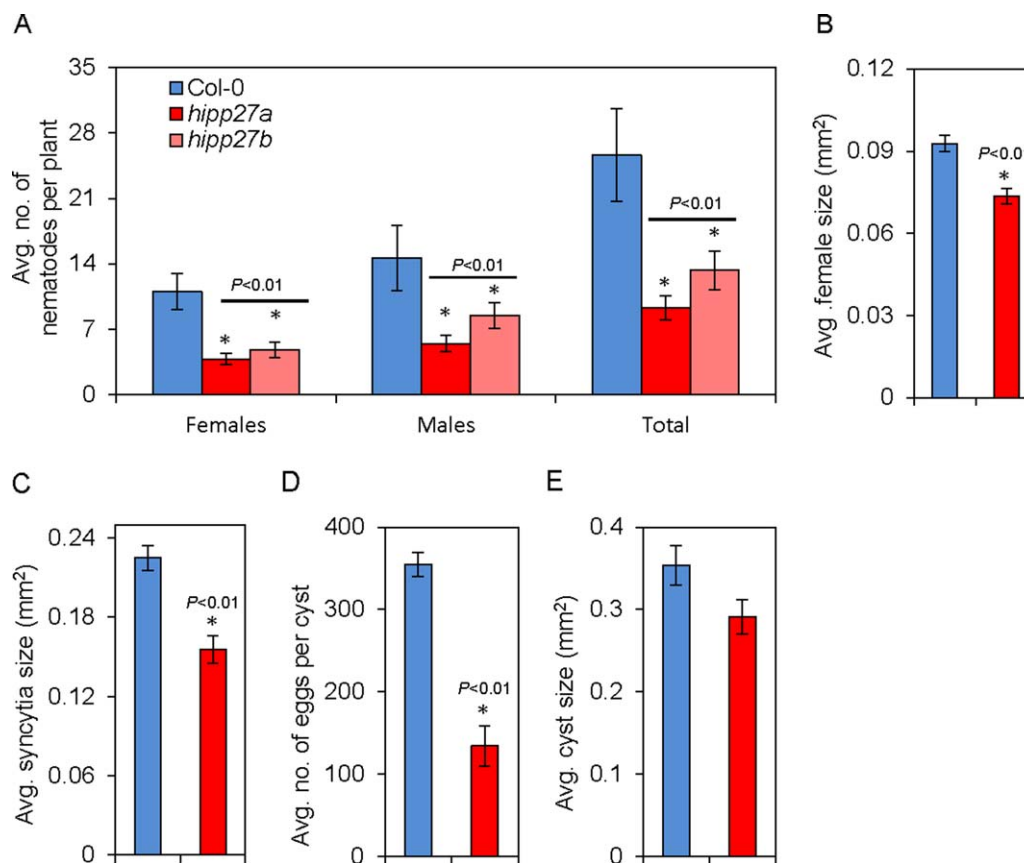
Fig. 2 Loss of function of *HIPP27* decreases Arabidopsis susceptibility to *Heterodera schachtii*. (A) Average number of nematodes per plant present in Col-0 ($n = 26$), *hipp27a* ($n = 45$) and *hipp27b* ($n = 36$) mutant lines at 14 days post-infection (dpi). (B) Average sizes of female nematodes in Col-0 ($n = 181$) and *hipp27a* ($n = 174$) at 14 dpi. (C) Average sizes of plant syncytia in Col-0 ($n = 181$) and *hipp27a* ($n = 174$) at 14 dpi. (D) Average number of eggs per cyst in Col-0 ($n = 66$) and *hipp27a* ($n = 56$) at 42 dpi. (E) Average cyst sizes in Col-0 ($n = 128$) and *hipp27a* ($n = 133$) at 42 dpi. (A–E) Bars represent mean $\pm$ standard error (SE). Asterisks represent statistically significant difference from corresponding Col-0 value (*t*-test, $*P < 0.05$).

difference in average dry weight, average flowering time, average root length or average plant height in the mutant compared with the control (Fig. S4A–D, see Supporting Information).

To analyse the changes in *hipp27* with regard to nematode susceptibility, we performed infection assays in which several susceptibility parameters were measured. The average number of females, a commonly accepted parameter indicating nematode susceptibility under *in vitro* conditions, was strongly reduced in both *hipp27a* (60%, $P < 0.01$) and *hipp27b* (40%, $P < 0.01$) compared with the control (Fig. 2A). In addition, the average numbers of males (*hipp27a*, 58%, $P < 0.01$; *hipp27b*, 48%, $P < 0.01$) and average total number of nematodes (*hipp27a*, 50%, $P < 0.01$; *hipp27b*, 55%, $P < 0.01$) were also significantly reduced in *hipp27* compared with Col-0 (Fig. 2A). Further susceptibility parameters, such as the average sizes of the female and the syncytium, were measured only for *hipp27a* and were also significantly reduced in *hipp27a* ($P < 0.01$) compared with Col-0 (Fig. 2B,C). For field-grown crops, the most common susceptibility parameters were the average number of eggs per cyst and

average size of cysts. We found that the average number of eggs per cyst was reduced significantly in *hipp27a* compared with Col-0 (Fig. 2D). Together, these results suggest that HIPP27 plays a vital role in cyst nematode parasitism.

Because loss of function of *HIPP27* resulted in a significant decrease in susceptibility to beet cyst nematodes, we hypothesized that overexpression of this gene might increase susceptibility to nematodes. To test this, we produced transgenic lines expressing *HIPP27* under the control of a constitutive promoter in either the Col-0 (*OXHIPP27*-L1 and *OXHIPP27*-L2) or *hipp27*a (*OXHIPP27*/*hipp27a*-L1 and *OXHIPP27*/*hipp27a*-L2) background. We confirmed the increase in transcript abundance in the homozygous lines by qRT-PCR (Fig. 3A) and performed an infection assay. We found that there was no significant change in average female size and syncytium size in these lines compared with the control ($P > 0.05$) (Fig. 3B,C). However, the average number of female nematodes per plant was significantly higher in the *OXHIPP27* lines (L1 = 13.68 $\pm$ 2.09, $P < 0.01$; L2 = 10.85 $\pm$ 1.91, $P = 0.02$) as well as one of the *OXHIPP27*/*hipp27a* lines
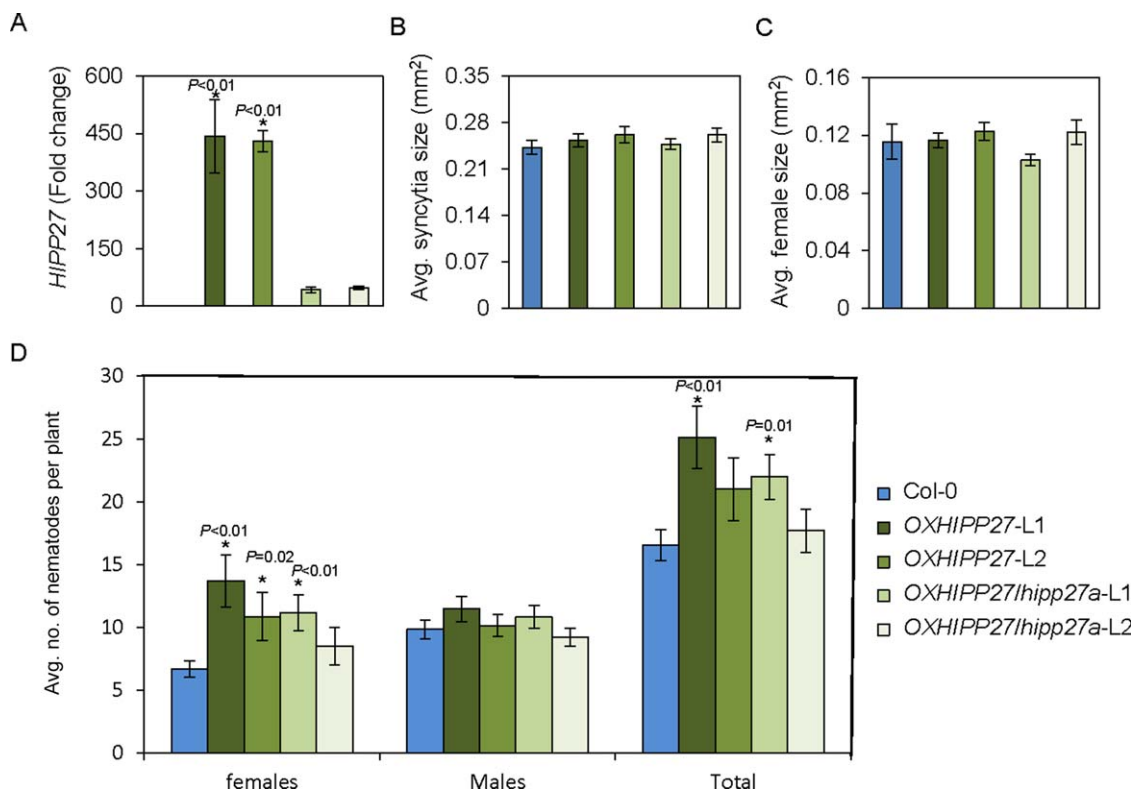
Fig. 3 Overexpression of *HIPP27* leads to increased susceptibility to *Heterodera schachtii*. (A) Quantitative reverse transcription-polymerase chain reaction (qRT-PCR) confirmation of the increase in *HIPP27* transcript in overexpression lines of the Col-0 (*OXHIPP27*) or *hipp27a* (*OXHIPP27/hipp27a*) background (*n* = 3). (B, C) Average sizes of syncytia (B) and female nematodes (C) in Col-0 (*n* = 77) and *HIPP27* (*OXHIPP27/L1*, *n* = 75; *OXHIPP27/L2*, *n* = 68; *OXHIPP27hipp27a/L1*, *n* = 90; *OXHIPP27hipp27a/L2*, *n* = 75) overexpression lines at 14 days post-infection (dpi). (D) Average number of nematodes per plant present in Col-0 (*n* = 40) and *HIPP27* overexpression lines (*OXHIPP27/L1*, *n* = 24; *OXHIPP27/L2*, *n* = 28; *OXHIPP27hipp27a/L1*, *n* = 26; *OXHIPP27hipp27a/L2*, *n* = 24) at 14 dpi. (A–D) Bars represent mean ± standard error (SE). Asterisks denote significant difference from corresponding Col-0 value (*t*-test, *$P < 0.05$).

(L1 = 11.15 ± 1.43, $P < 0.01$) compared with Col-0 (6.75 ± 0.65) (Fig. 3D). Moreover, we also found a significant increase in the total number of nematodes in one *OXHIPP27* line (L1 = 25.13 ± 2.46, $P < 0.01$) and one *OXHIPP27/hipp27a* line (L1 = 21.96 ± 1.43, $P = 0.01$) compared with the control (16.52 ± 1.21) (Fig. 3D). Together, these data suggest that the expression of *HIPP27* is activated on cyst nematode infection and is required for proper syncytium and nematode development.

Loss of function of *HIPP27* does not lead to increased susceptibility to other pathogens

We wanted to determine whether the *hipp27* mutant exhibits increased susceptibility to other pathogens. Therefore, we performed infection assays using the gall-forming nematode *Meloidogyne javanica* and the necrotrophic fungus *Botrytis cinerea*. We did not observe differences between the wild-type and mutant in the average size of necrotic lesions caused by *B. cinerea* (Fig. 4A). In addition, we found that the number of galls formed by *M. javanica* in *hipp27a* did not differ significantly relative to that

in Col-0 controls ($P > 0.05$) (Fig. 4B). To further rule out a putative role for HIPP27 during gall formation, we compared the diameters of the galls in the wild-type and *hipp27a* mutant lines, finding no significant differences between them (Fig. 4C). Moreover, the reproduction of the root-knot nematodes, measured as the number of egg masses per gall, was statistically unaffected in *hipp27a* ($P > 0.05$) (Fig. 4D). Together, these data point to a cyst nematode-specific role of *HIPP27* in supporting parasitism.

Loss of function of *HIPP27* does not impair plant basal defence

To investigate whether the reduced susceptibility of *hipp27a* plants to *H. schachtii* is a result of altered plant defence responses, we measured the reactive oxygen species (ROS) levels induced over a 60-min period on treatment of leaves with a well-known immunopeptide, flg22. We did not observe significant changes in ROS levels (Fig. 5A,B), indicating that the *hipp27a* mutant does not have impaired plant basal defence responses. To further confirm this finding, we performed qRT-PCR analysis to
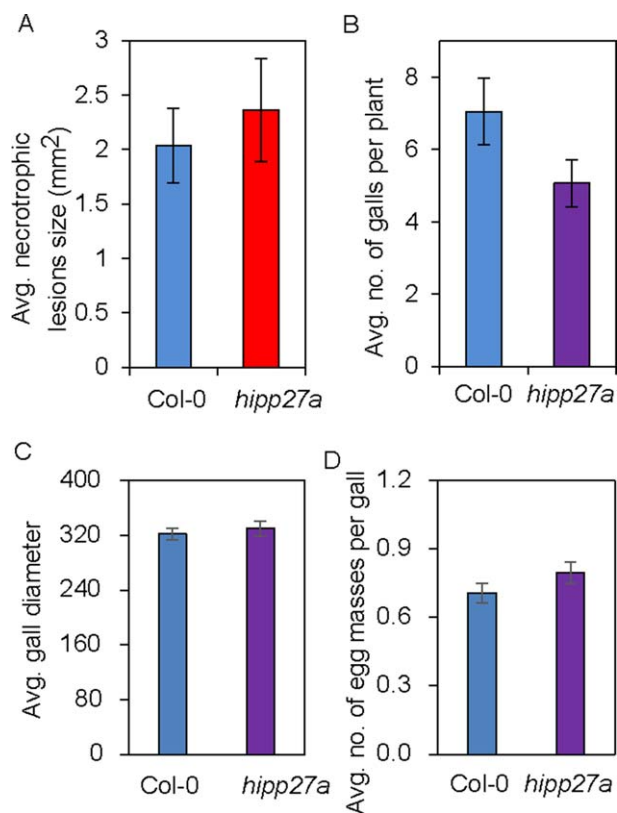
Fig. 4 Loss of function of *HIPP27* does not alter the susceptibility to other pathogens. (A) Average size of lesions induced by *Botrytis cinerea* in Col-0 ($n = 21$) and *hipp27a* ($n = 14$) lines. (B) Average number of galls per plant in Col-0 ($n = 55$) and *hipp27* ($n = 60$) mutant at 21 days post-infection (dpi) with *Meloidogyne javanica*. (C) Gall size calculated as the diameter of galls from Col-0 ($n = 36$) and *hipp27* ($n = 37$) at 14 dpi with *M. javanica*. (D) Number of egg masses formed per gall by *M. javanica* in Col-0 ($n = 363$) and *hipp27a* ($n = 304$) 2 months after infection. Statistical analysis was performed using Student's *t*-test (no significant differences from Col-0 were observed). Bars represent mean ± standard error (SE).

examine the expression of a few plant basal defence marker genes in uninfected shoots: *PR1* and *PR2* are induced by salicylic acid, *PDF1.2* and *HEL1* are marker genes for jasmonic acid signalling, and *ERF6* and *ACS2* are involved in ethylene signalling. The expression levels of all marker genes in the *hipp27* mutant were similar to those of Col-0 (Fig. 5C). These results reinforce the conclusion that *HIPP27* has a specific role in the interaction with cyst nematodes, as an increase in plant basal defence would lead to resistance to other pathogens (Fig. 4A–D).

Loss of function of *HIPP27* causes physiological or metabolic abnormalities

Finally, we examined the anatomical and ultrastructural organization of syncytia induced by the beet cyst nematode in roots of wild-type Col-0 and *hipp27a* mutant plants (Fig. 6). Comparison

of light microscopy images of sections taken through similar regions of nematode-induced syncytia showed no apparent differences between the syncytia induced in the two genotypes (Fig. 6A–D versus 6E–H). Next to the nematode head, the syncytia were relatively small on cross-sections and cells not incorporated into them divided at different planes, forming groups of neoplastic cells (Fig. 6A,C,E,G), similar to those described by Sobczak *et al.* (1997). The extent of destruction around the nematode head was also similar in both plant genotypes (Fig. 6A,C,E,G). Sections from the middle and the widest regions of syncytia (distant from the nematode head) showed that, if the syncytium had been induced in young roots without fully differentiated primary xylem, it occupied the central position inside the vascular cylinder and became surrounded by regularly dividing pericyclic cells forming the periderm, a secondary cover tissue (Fig. 6B,F). However, if the syncytium had been induced in the root region in which the primary xylem was fully differentiated, it developed the primary xylem on only one side, whereas secondary xylem elements differentiated on the opposite side (Fig. 6D,H). In both cases, the pericyclic cells divided and formed periderm around the entire vascular cylinder (Fig. 6B,D,F,H). No visible differences in the extent of syncytial element hypertrophy or the number and size of cell wall openings were evident, indicating that the anatomical structure of syncytia induced in the *hipp27* mutant was undisturbed (Fig. 6A–H), although their dimensions were smaller compared with Col-0 (Fig. 2).

At the ultrastructural level, syncytia induced in Col-0 and *hipp27*a plants were similar at 5 dpi (Fig. 6I,K). Their cytoplasm proliferated and became electron dense, with numbers of plastids, mitochondria and endoplasmic reticulum structures increasing, whereas central vacuoles disappeared. Only a few syncytial plastids contained very small starch grains. However, serial sectioning of syncytia showed that syncytia induced in *hipp27a* roots often differed in their ultrastructure along their axis. In the region close to the nematode head and at the leading edge (the most remote part of the syncytium), syncytia had typical ultrastructural organization (Fig. 6K). By contrast, in the middle region of the syncytium, the cytoplasm was relatively electron translucent, endoplasmic reticulum structures were weakly developed and large starch grains were formed in numerous syncytial plastids and plastids of peridermal cells next to the syncytium (Fig. 6L). In samples collected at 10 dpi, syncytial protoplasts had typical ultrastructure in syncytia induced in wild-type Col-0 plants (Fig. 6J). Here again, small starch grains were present in only a few syncytial plastids and were absent in cells surrounding the syncytium. By contrast, starch grains were frequently present in peridermal plastids next to syncytia induced in *hipp27a* roots (Fig. 6M,N). Inside syncytia, plastids present in regions with well-developed endoplasmic reticulum usually did not contain starch grains (Fig. 6M), whereas plastids present in regions with electron
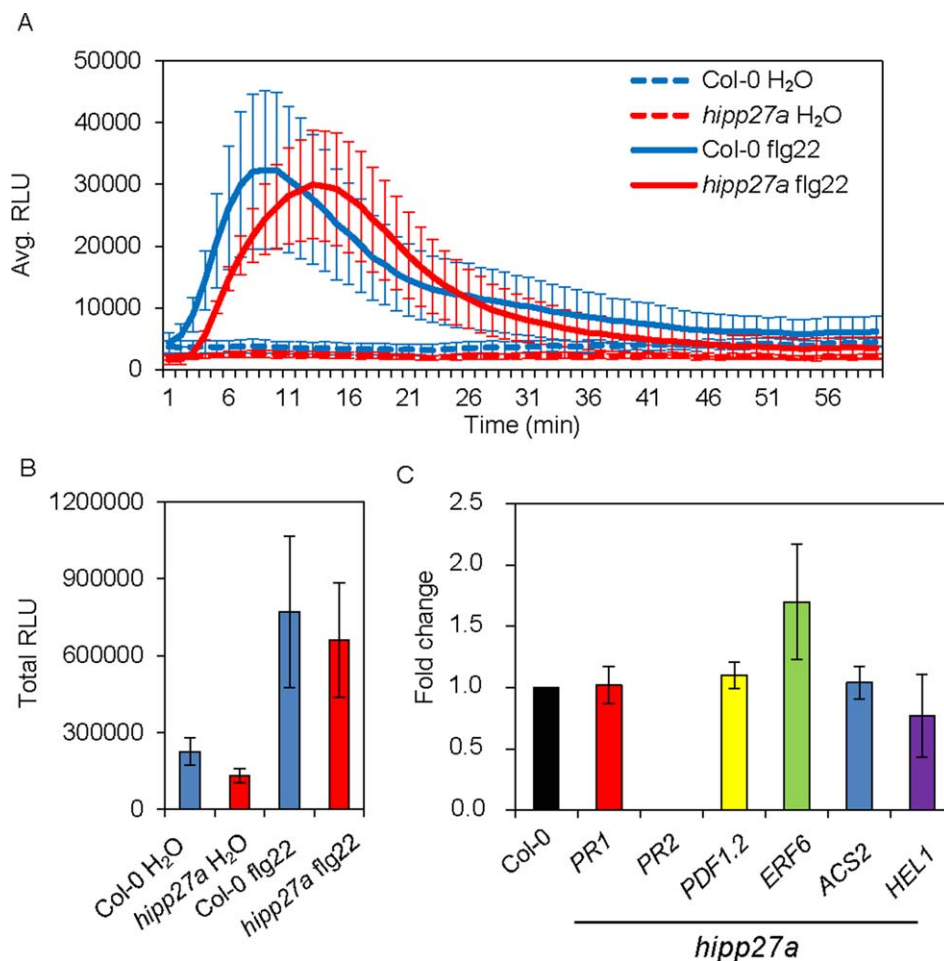
Fig. 5 Loss of function of *HIPP27* does not impair plant basal defence. (A) Reactive oxygen species (ROS) burst induced by flg22 during 60 min of measurement in Col-0 and *hipp27a* mutant expressed in relative light units (RLU) ($n = 3$). (B) Total RLU of ROS during 60 min of exposure to flg22 in Col-0 and *hipp27a* mutant ($n = 3$). (C) Quantitative reverse transcription-polymerase chain reaction (qRT-PCR) gene expression analysis of defence-related genes in uninfected shoots of Col-0 and *hipp27a* mutant ($n = 3$). Statistical analysis was performed using Student's *t*-test (no significant differences from Col-0 were observed). Bars represent mean ± standard error (SE).

translucent cytoplasm and poorly developed endoplasmic reticulum usually contained large starch grains (Fig. 6N,O). Some of these plastids acquired enormously large sizes (Fig. 6O) and could be clearly recognized even on anatomical sections (Fig. 6H). Taken together, our ultrastructural analysis shows that loss of function of HIPP27 leads to physiological and metabolic abnormalities, including the accumulation of large starch grains.

CONCLUSION

This study represents the first investigation of the role of an HIPP family protein in plant–nematode interactions. We showed that the expression of *HIPP27* is specifically and highly upregulated in syncytia induced by *H. schachtii* in Arabidopsis roots. The strong GUS expression driven by the *HIPP27* promoter inside the syncytium points to the involvement of *HIPP27* in the establishment and development of syncytia. Indeed, the analysis of loss-of-function mutants and overexpression lines showed that *HIPP27* expression supports infection of the host roots by the beet cyst nematode. In contrast with its expression in cyst nematode-induced syncytia, *HIPP27* expression was not differentially

regulated in feeding sites induced by root-knot nematodes (Cabrera *et al*., 2014). These observations indicate that the role of *HIPP27* in facilitating parasitism is restricted to that of cyst nematodes. This hypothesis is further supported by results from pathogenicity assays with *M. javanica* and *B. cinerea*, in which we did not observe any significant difference in susceptibility between Col-0 and the *hipp27* mutant.

HIPP27 belongs to Cluster IV of the HIPP family in Arabidopsis, which is notable for the presence of a conserved aspartic acid (Asp) residue preceding the metal binding motif (CysXXCys). Notably, the expression of *HIPP27* in yeast confers a slight increase in cadmium (Cd) resistance to a Cd-sensitive yeast strain, probably as a result of binding of Cd by HIPP27 in the cytosol (Tehseen *et al*., 2010). Several HIPP family members, including HIPP26 and HIPP27, have been shown to interact via the HMA domain with the drought stress-related zinc finger transcription factor 29 (ATHB29) and UBIQUITIN-SPECIFIC PROTEASE 16 (UBP16) (Barth *et al*., 2009; Zhao *et al*., 2013). In addition, *hipp26* mutants display altered expression of ATHB29-regulated dehydration response genes compared with the wild-type (Barth *et al*., 2009). Whether HIPP27 plays a similar role in ATHB29-mediated
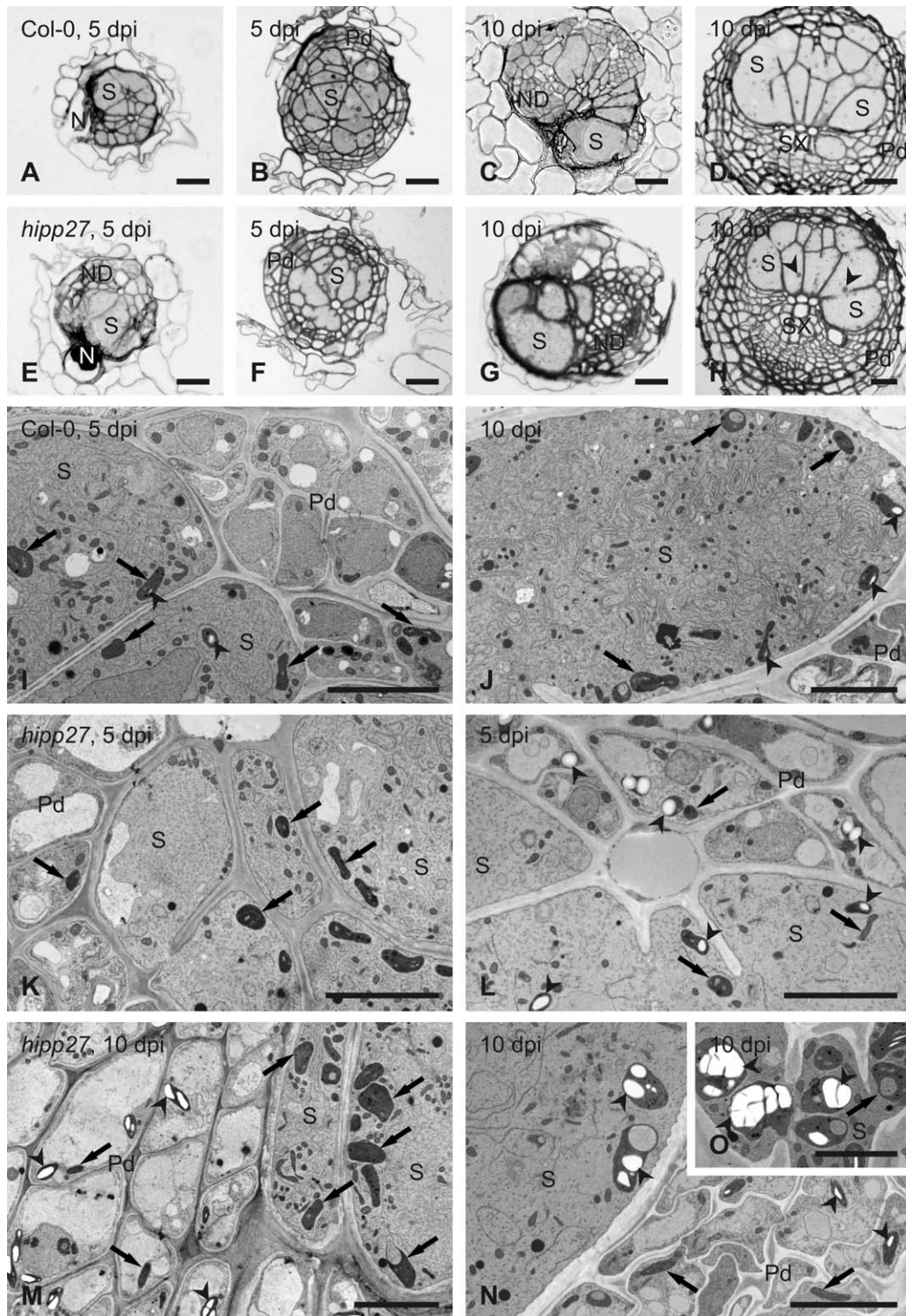
Fig. 6 Loss of function of *HIPP27* causes physiological or metabolic abnormalities. Light (A–H) and transmission electron (I–O) microscopy images of cross-sections of syncytia at 5 days post-infection (dpi) (A, B, E, F, I, K and L) and 10 dpi (C, D, G, H, J and M–O) induced in roots of Col-0 wild-type plants (A–D, I and J) and *hipp27a* mutant (E–H and K–O). Light microscopy images were taken close to the nematode head (A, C, E and G) or through the widest regions of syncytia (B, D, F and H). Arrowheads indicate selected starch grains in plastids; arrows point to plastids. N, nematode; ND, neoplastic divisions; Pd, periderm; S, syncytium; SX, secondary xylem. Scale bars: 20 μm (A–H), 5 μm (I–O).

gene regulation remains to be explored. Previous microarray analysis using microaspirated *H. schachtii* syncytium protoplasts has shown that the expression of both *ATHB29* and *UBP16* is downregulated in syncytia relative to uninfected control roots. By contrast, *HIPP27* is highly upregulated in syncytia (Szakasits *et al.*, 2009). These observations make it likely that HIPP27 acts independently of ATHB29 to regulate infection by *H. schachtii*.

Our data showed no difference in the activation of the ROS burst or in the expression of defence genes between Col-0 and *hipp27a* mutant lines. Based on these results, we propose that the expression of *HIPP27* is required for the maintenance of the optimal development or functioning of the syncytium. This hypothesis is supported by the observation that the syncytium size was significantly reduced in *hipp27a* compared with Col-0. The syncytium is a strong metabolic sink that serves as the only source of nutrients for developing nematodes, and the maintenance of metal homeostasis in the syncytium must be tightly regulated. Considering the role of HIPP family members as metallochaperones, it is plausible that HIPP27 functions in metal transport and homeostasis in the syncytium. Indeed, microscopic observations confirmed that the lack of HIPP27 protein does not influence the general developmental pattern of syncytia, but causes physiological or metabolic disorders, leading to the accumulation of phloem-provided saccharides as starch grains in peridermal and syncytial plastids. These sugars may become unavailable to parasitic juveniles, leading to their disturbed development. Hofmann *et al.* (2008) have shown that the number of starch grains increases in syncytia during nematode moult, when no food is taken up by the associated juvenile, as well as in degraded syncytia of adult males and prematurely degraded syncytia associated with females. As no clearly degraded syncytia were found in our experiments, it can be speculated that starch accumulation and its potential unavailability for the nematodes are very early features of syncytium degradation, and that these processes impair the development of beet cyst nematodes on *hipp27* roots. However, further work is required to elucidate the precise role of HIPP27 in cyst nematode parasitism.

In conclusion, we have identified *HIPP27* as a host susceptibility gene whose deletion reduces plant susceptibility to cyst nematodes without increasing susceptibility to other pathogens. The lack of developmental phenotypes in *hipp27* plants highlights the potential of using *HIPP27* in the breeding of nematode-resistant crop plants.

EXPERIMENTAL PROCEDURES

Plant growth and beet cyst nematode infection

Arabidopsis thaliana seeds were sterilized for 5 min with 1.2% NaClO, followed by three consecutive washes with autoclaved double-distilled H_2O. Sterilized seeds were sown in KNOP medium, and 12-day-old plants were infected with 70–80 surface-sterilized second-stage juveniles (J2s). For surface sterilization, hatched J2s were washed with 0.05% $HgCl_2$, followed by three consecutive washes with autoclaved double-distilled H_2O (Sijmons *et al.*, 1991). Two weeks after inoculation, nematode susceptibility parameters, such as the average number of females, average number of males and average number of total nematodes per plant, were quantified under a Leica S4E stereomicroscope (Leica Microsystems, Wetzlar, Germany), and average female and syncytium sizes were measured under a Leica M 165C stereomicroscope (Leica Microsystems) equipped with Leica LAS v4.3 image analysis software (Leica Microsystems). Cyst size and the average number of eggs per cyst were measured and counted at 42 days after inoculation. All infection assays were repeated at least three times and 10–20 plants were used in each repetition. The data from all individual plants from three experiments were combined to a single mean.

Infection assays with *M. javanica* and *B. cinerea*

Infection assays using *M. javanica* were performed as described previously (Cabrera *et al.*, 2014). In brief, Arabidopsis plants were grown aseptically on 0.3% Gamborg's medium (Gamborg *et al.*, 1968) supplemented with 1.5% (w/v) sucrose for 14 days. Fourteen-day-old plants were inoculated with 70–100 *M. javanica* J2s per plant. The infected plants were incubated at 23 °C and 16 h : 8 h light : dark photoperiod. The number of galls was counted at 21 dpi. Gall diameters were measured at 14 dpi using ImageJ. The infection assays with *B. cinerea* were performed as described previously (Lozano-Torres *et al.*, 2014). In brief, 5-μL drops of fungal spores at a concentration of 5×10^5 were inoculated onto 4-week-old Arabidopsis plants grown in soil under glasshouse conditions. The infected plants were incubated for 3 days in the dark at 20 °C and 100% relative humidity. Plant susceptibility was estimated by measuring the sizes of necrotic areas at 3 dpi in the same manner as used to measure the sizes of syncytia or females (Siddique *et al.*, 2014b).

Genotyping and expression analysis of the mutants

Arabidopsis SAIL lines (*hipp27a*, SAIL_167_B06; *hipp27b*, SAIL_675_E09) were ordered from the Nottingham Arabidopsis Stock Centre (NASC), Nottingham, UK. Homozygosity of the lines was tested by extracting plant DNA using the cetyltrimethylammonium bromide (CTAB) method, after which PCR with SAIL primers was conducted to confirm the T-DNA insertions in these lines. PCR was performed on a C100™ Thermal Cycler (Bio-Rad Laboratories, USA). Visual observation of homozygosity and expression analysis were performed using Gel Doc™ (Bio-Rad Laboratories, Hercules, California, USA), together with Lab 3.0 software. The primer sequences are listed in Table S1 (see Supporting Information).

qRT-PCR gene expression analysis

To measure transcript abundance, plants were grown in Knop medium, and RNA from Col-0 and mutant or overexpression leaves was extracted using Nucleospin RNA XS (Macherey-Nagel, Düren, Germany) according to the manufacturer's protocol. RNA was extracted from a pool of three to four plants. This RNA was then used to synthesize first-strand cDNA—a procedure repeated three times in three independent experiments. The RNA concentration was measured with a NanoDrop (Thermo Fisher

Scientific, Waltham, MA, USA), and cDNA was prepared using a High Capacity cDNA Reverse Transcript kit (Life Technologies, Waltham, MA, USA). Transcript abundance was measured on a StepOnePlus Real-Time PCR System (Applied Biosynthesis, Waltham, MA, USA) as described by Pfaffl (2001); *18S* and *UBP22* were used as internal controls as recommended previously (Hofmann and Grundler, 2007). Expression in each experiment was measured in three technical replicates.

Plant phenotyping

Phenotypic parameters of Arabidopsis Col-0 and *hipp27a* lines were measured using soil-grown plants in a glasshouse and plants grown in Petri dishes on KNOP medium under sterile conditions. Measurements were conducted under a Leica M 165C stereomicroscope (Leica Microsystems) equipped with Leica LAS v4.3 image analysis software (Leica Microsystems), as described previously, or manually using a ruler and balance following standard phenotyping protocols (Bolle, 2009). The experiments were repeated at least three times and data from all individual plants from all three experiments were combined to a single mean.

Gateway cloning and plant transformation

Gateway cloning was used to clone the *HIPP27* promoter (472 bp upstream of *HIPP27*) and to clone the *HIPP27* CDS into the pDONR207 vector. Briefly, primers with attB extensions were designed and the PCR product was inserted into the pDONR207 vector using Gateway® BP Clonase[TM] II Enzyme mix (Invitrogen, Waltham, MA, USA). The pEntry207 vector was transformed into *Escherichia. coli* (DH5α) competent cells using the heat shock method. The pEntry207 vector was then extracted using a Nucleospin® plasmid extraction kit (Macherey-Nagel), and homologous recombination of the gene or promoter into the destination vector was performed using Gateway® LR Clonase[TM] II Enzyme mix (Invitrogen). For *HIPP27:GUS*, the destination vector was pMDC162; for *HIPP27:GFP*, the destination vector was pMDC107; for *35S:HIPP27*, the destination vector was pMDC32 (Curtis and Grossniklaus, 2003). Arabidopsis plants were transformed via the floral dip method (Clough and Bent, 1998).

GUS staining

The *HIPP27:GUS* reporter construct was introduced into the Col-0 background, and homozygous lines for the reporter gene were selected in subsequent generations using selection marker genes and genotyping. Histochemical GUS analysis was performed according to Siddique *et al.* (2009). Briefly, the *HIPP27:GUS* lines were grown in Knop medium as described above. The roots were submerged in X-Gluc (5-Bromo-4-chloro-1*H*-indol-3-yl β-D-glucopyranosiduronic acid) for 6 h at 37 °C at 1, 3, 5 and 10 dpi. The number of stained syncytia was counted, and photographs were taken under a DMI 4000B microscope (Leica Microsystems).

Nicotiana benthamiana infiltration assay

The coding region of *HIPP27* without the stop codon was amplified using Gateway forward and reverse primers as given in Table S1. The amplified product was cloned into pDONR207 using Gateway® BP Clonase[TM] II Enzyme mix (Invitrogen). The gene was shuttled into the destination vector, i.e. pMDC83, using Gateway® LR Clonase[TM] II Enzyme mix (Invitrogen). The

HIPP27:GFP construct was transiently expressed in the epidermis of 6-week-old *N. benthamiana* leaves under the control of the 35S promoter. The GFP fluorescence was observed under an LSM 710 confocal microscope at 3 days after infiltration (Carl Zeiss, Oberkochen, Germany). The wavelength was 488 nm for excitation and 514–550 nm for emission.

Oxidative burst assay

ROS production was measured on a 96-well illuminometer (Mithras LB 940; Berthold Technologies, Bad Wildbad, Germany) according to Mendy *et al.* (2017). Briefly, leaf discs, 0.5 cm in diameter, were cut from 12-day-old Arabidopsis plants and incubated in double-distilled H_2O for 12 h in the dark. Each leaf disc was placed into the well of a 96-well plate containing 15 μL of 20 μg/mL horseradish peroxidase and 35 μL of 10 mM 8-amino-5-chloro-2,3-dihydro-7-phenyl(3,4-d) pyridazine sodium salt (L-012, Wako Chemicals, Neuss, Germany). ROS bursts were induced with 50 μL of flg22 (100 μM), with double-distilled H_2O used as a negative control. Light emission was measured for 60 min, and results were obtained using the software supplied with the instrument.

Anatomical and ultrastructural analyses

Root segments containing syncytia were dissected from *in vitro*-grown and *H. schachtii*-inoculated Arabidopsis Col-0 and *hipp27a* plants at 5 and 10 dpi. They were chemically fixed in a mixture of aldehydes and processed for microscopic examinations as described by Golinowski *et al.* (1996) and Sobczak *et al.* (1997). After embedding in epoxy resin, the samples were serially sectioned for light microscopy examinations; at selected places, ultrathin sections were taken for transmission electron microscopy (Siddique *et al.*, 2014b). The images obtained were cropped, resized and adjusted for similar contrast and brightness using Adobe Photoshop software. Three syncytia induced in *hipp27a* roots at 5 dpi were sectioned and examined. In two of them, starch grains and regions with reduced numbers of endoplasmic reticulum structures were found, whereas, in the third, no such features were observed. In the case of 10-dpi syncytia, five samples were examined and all displayed starch grains and regions with reduced numbers of endoplasmic reticulum structures.

Bioinformatics analysis

To select the 100 most highly upregulated genes in the 5 + 15-dpi syncytium, the NEMATIC program was used (Cabrera *et al.*, 2014). Orthologues of Arabidopsis genes were identified using The *Beta vulgaris* Resource (http://bvseq.mol gen.mpg.de/index.shtml); Arabidopsis genes sharing at least 60% amino acid sequence identity with sugar beet and without additional homologues were selected. Primers were designed using primer3 online software (http://bioinfo.ut.ee/primer3-0.4.0/). SAIL primers were obtained from the SALK website (http://signal.salk.edu/tdnaprimers.2.html). A list of all primers is presented in Table S1.

Statistical data analysis

Results are presented as the mean $\pm$ standard error (SE) from at least three independent experiments. Statistically significant differences were defined using Microsoft Office Excel and extension XL Statistics with Student's *t*-test ($P < 0.05$).

ACKNOWLEDGEMENTS

REFERENCES

de Abreu-Neto, J.B., Turchetto-Zolet, A.C., de Oliveira, L.F.V., Zanettini, M.H.B. and Margis-Pinheiro, M. (2013) Heavy metal-associated isoprenylated plant protein (HIPP): characterization of a family of proteins exclusive to plants. *FEBS J.* **280**, 1604–1616.

Barth, O., Vogt, S., Uhlemann, R., Zschiesche, W. and Humbeck, K. (2009) Stress induced and nuclear localized HIPP26 from *Arabidopsis thaliana* interacts via its heavy metal associated domain with the drought stress related zinc finger transcription factor ATHB29. *Plant Mol. Biol.* **69**, 213–226.

Bolle, C. (2009) Phenotyping of Arabidopsis mutants for developmental effects of gene deletions. *Methods Mol. Biol.* **479**, 17–34.

Cabrera, J., Bustos, R., Favery, B., Fenoll, C. and Escobar, C. (2014) NEMATIC: a simple and versatile tool for the *in silico* analysis of plant–nematode interactions. *Mol. Plant Pathol.* **15**, 627–636.

Clough, S.J. and Bent, A.F. (1998) Floral dip: a simplified method for Agrobacterium-mediated transformation of *Arabidopsis thaliana. Plant J.* **16**, 735–743.

Curtis, M.D. and Grossniklaus, U. (2003) A gateway cloning vector set for high-throughput functional analysis of genes in planta. *Plant Physiol.* **133**, 462–469.

Dohm, J.C., Minoche, A.E., Holtgräwe, D., Capella-Gutiérrez, S., Zakrzewski, F., Tafer, H., Rupp, O., Sörensen, T.R., Stracke, R., Reinhardt, R., Goesmann, A., Kraft, T., Schulz, B., Stadler, P.F., Schmidt, T., Gabaldón, T., Lehrach, H., Weisshaar, B. and Himmelbauer, H. (2014) The genome of the recently domesticated crop plant sugar beet (*Beta vulgaris*). *Nature*, **505**, 546–549.

Elashry, A., Okumoto, S., Siddique, S., Koch, W., Kreil, D.P. and Bohlmann, H. (2013) The AAP gene family for amino acid permeases contributes to development of the cyst nematode *Heterodera schachtii* in roots of Arabidopsis. *Plant Physiol. Biochem.* **70**, 379–386.

Gamborg, O.L., Miller, R.A. and Ojima, K. (1968) Nutrient requirements of suspension cultures of soybean root cells. *Exp. Cell Res.* **50**, 151–158.

Gardner, M., Verma, A. and Mitchum, M.G. (2015) Emerging roles of cyst nematode effectors in exploiting plant cellular processes. In: *Plant Nematode Interactions — A View on Compatible Interrelationships* (Escobar, C. and Fenoll, C., eds), pp. 259–291. Oxford: Elsevier.

Golinowski, W., Grundler, F.M.W. and Sobczak, M. (1996) Changes in the structure of *Arabidopsis thaliana* during female development of the plant-parasitic nematode *Heterodera schachtii. Protoplasma*, **194**, 103–116.

Habash, S.S., Radakovic, Z.S., Vankova, R., Siddique, S., Dobrev, P., Gleason, C., Grundler, F.M.W. and Elashry, A. (2017) *Heterodera schachtii* tyrosinase-like protein – a novel nematode effector modulating plant hormone homeostasis. *Sci. Rep.* **7**, 6874.

Hewezi, T., Juvale, P.S., Piya, S., Maier, T.R., Rambani, A., Rice, J.H., Mitchum, M.G., Davis, E.L., Hussey, R.S. and Baum, T.J. (2015) The cyst nematode effector protein 10A07 targets and recruits host posttranslational machinery to mediate its nuclear trafficking and to promote parasitism in Arabidopsis. *Plant Cell*, **27**, 891–907.

Hofmann, J. and Grundler, F.M. (2007) Identification of reference genes for qRT-PCR studies of gene expression in giant cells and syncytia induced in *Arabidopsis thaliana* by *Meloidogyne incognita* and *Heterodera schachtii. Nematology*, **9**, 317–323.

Hofmann, J., Szakasits, D., Blochl, A., Sobczak, M., Daxbock-Horvath, S., Golinowski, W., Bohlmann, H. and Grundler, F.M.W. (2008) Starch serves as carbohydrate storage in nematode-induced syncytia. *Plant Physiol.* **146**, 228–235.

Hofmann, J., El Ashry, A., Anwar, S., Erban, A., Kopka, J. and Grundler, F.M.W. (2010) Metabolic profiling reveals local and systemic responses of host plants to nematode parasitism. *Plant J.* **62**, 1058–1071.

Hütten, M., Geukes, M., Misas-Villamil, J.C., van der Hoorn, R.A.L., Grundler, F.M.W. and Siddique, S. (2015) Activity profiling reveals changes in the diversity and activity of proteins in Arabidopsis roots in response to nematode infection. *Plant Physiol. Biochem.* **97**, 36–43.

Jones, J.T., Haegeman, A., Danchin, E.G.J., Gaur, H.S., Helder, J., Jones, M.G.K., Kikuchi, T., Manzanilla-López, R., Palomares-Rius, J.E., Wesemael, W.M.L. and Perry, R.N. (2013) Top 10 plant-parasitic nematodes in molecular plant pathology. *Mol. Plant Pathol.* **14**, 946–961.

Lozano-Torres, J.L., Wilbers, R.H.P., van Warmerdam, S., Finkers-Tomczak, A., van Schaik, C.C., Overmars, H., Bakker, J., Goverse, A. and Smant, G. (2014) Secreted venom allergen-like proteins of plant-parasitic nematodes modulate defence responses in host plants. *J. Nematol.* **46**, 196–197.

Mendy, B., Wang'ombe, M.W., Radakovic, Z.S., Holbein, J., Ilyas, M., Chopra, D., Holton, N., Zipfel, C., Grundler, F.M.W. and Siddique, S. (2017) Arabidopsis leucine-rich repeat receptor-like kinase NILR1 is required for induction of innate immunity to parasitic nematodes. *PLoS Pathog.* **13**, e1006284.

Pfaffl, M.W. (2001) A new mathematical model for relative quantification in real-time RT-PCR. *Nucleic Acids Res.* **29**, e45.

Sarris, P.F., Cevik, V., Dagdas, G., Jones, J.D.G. and Krasileva, K.V. (2016) Comparative analysis of plant immune receptor architectures uncovers host proteins likely targeted by pathogens. *BMC Biol.* **14**, 8.

Shah, S.J., Anjam, M.S., Mendy, B., Habash, S.S., Anwer, M.A., Lozano-Torres, J.L., Grundler, F.M.W. and Siddique, S. (2017) Damage-associated responses of the host contribute to defence against cyst nematodes but not root-knot nematodes. *J. Exp. Bot.* **68**, 5949–5960.

Siddique, S., Endres, S., Atkins, J.M., Szakasits, D., Wieczorek, K., Hofmann, J., Blaukopf, C., Urwin, P.E., Tenhaken, R., Grundler, F.M.W., Kreil, D.P. and Bohlmann, H. (2009) Myo-inositol oxygenase genes are involved in the development of syncytia induced by *Heterodera schachtii* in Arabidopsis roots. *New Phytol.* **184**, 457–472.

Siddique, S., Endres, S., Sobczak, M., Radakovic, Z.S., Fragner, L., Grundler, F.M.W., Weckwerth, W., Tenhaken, R. and Bohlmann, H. (2014a) Myo-inositol oxygenase is important for the removal of excess myo-inositol from syncytia induced by *Heterodera schachtii* in Arabidopsis roots. *New Phytol.* **201**, 476–485.

Siddique, S., Matera, C., Radakovic, Z.S., M.H.S., Hasan, M.H., Gutbrod, P., Rozanska, E., Sobczak, M., Torres, M.A. and Grundler, F.M. (2014b) Parasitic worms stimulate host NADPH oxidases to produce reactive oxygen species that limit plant cell death and promote infection. *Sci. Signal.* **7**, ra33.

Siddique, S., Radakovic, Z.S., De La Torre, C.M., Chronis, D., Novák, O., Ramireddy, E., Holbein, J., Matera, C., Hütten, M., Gutbrod, P., Anjam, M.S., Rozanska, E., Habash, S., Elashry, A., Sobczak, M., Kakimoto, T., Strnad, M., Schmülling, T., Mitchum, M.G. and Grundler, F.M.W. (2015) A parasitic nematode releases cytokinin that controls cell division and orchestrates feeding site formation in host plants. *Proc. Natl. Acad. Sci. USA*, **112**, 12 669–12 674.

Sijmons, P.C., Grundler, F.M.W., Mende, N., Burrows, P.R. and Wyss, U. (1991) *Arabidopsis thaliana* as a new model host for plant-parasitic nematodes. *Plant J.* **1**, 245–254.

Sobczak, M., Golinowski, W. and Grundler, F.M.W. (1997) Changes in the structure of *Arabidopsis thaliana* roots induced during development of males of the plant parasitic nematode *Heterodera schachtii. Eur. J. Plant Pathol.* **103**, 113–124.

Szakasits, D., Heinen, P., Wieczorek, K., Hofmann, J., Wagner, F., Kreil, D.P., Sykacek, P., Grundler, F.M.W. and Bohlmann, H. (2009) The transcriptome of syncytia induced by the cyst nematode *Heterodera schachtii* in Arabidopsis roots. *Plant J.* **57**, 771–784.

Tehseen, M., Cairns, N., Sherson, S. and Cobbett, C.S. (2010) Metallochaperone-like genes in *Arabidopsis thaliana. Metallomics*, **2**, 556–564.

Trudgill, D.L. (1967) Effect of environment on sex determination in *Heterodera rostochiensis. Nematologica*, **13**, 263–272.

Wyss, U. and Zunke, U. (1986) Observations on the behavior of second stage juveniles of *Heterodera schachtii* inside host roots. *Rev. Némathol.* **9**, 153–165.

Zhao, J., Zhou, H. and Li, X. (2013) UBIQUITIN-SPECIFIC PROTEASE16 interacts with a HEAVY METAL ASSOCIATED ISOPRENYLATED PLANT PROTEIN27 and modulates cadmium tolerance. *Plant Signal. Behav.* **8**, e25680.

Zschiesche, W., Barth, O., Daniel, K., Böhme, S., Rausche, J. and Humbeck, K. (2015) The zinc-binding nuclear protein HIPP3 acts as an upstream regulator of the

salicylate-dependent plant immunity pathway and of flowering time in *Arabidopsis thaliana. New Phytol.* **207**, 1084–1096.

SUPPORTING INFORMATION

Additional Supporting Information may be found in the online version of this article at the publisher's website:

Fig. S1 Cyst nematode infection assay in Col-0 and mutants of 10 selected candidate genes.

Fig. S2 Genotyping of *hipp27* mutant lines.

Fig. S3 Reverse transcription-polymerase chain reaction (RT-PCR) analysis of *HIPP27* expression in Col-0 and *hipp27* mutant lines.

Fig. S4 Phenotyping of Col-0 and *hipp27a* mutant line grown under different growth conditions.

Table S1 List of all primer sequences used in this study.